Received: 17 July 2022 | Revised: 17 August 2022 | Accepted: 22 August 2022

DOI: 10.1002/aoc.6879

RESEARCH ARTICLE

Applied Organometallic Chemistry WILEY

Schottky type photodiodes with organic Co-complex and Cd-complex interlayers

Adem Kocyigit[1] | **Ali Akbar Hussaini**[2] | **Murat Yıldırım**[2] | **Dursun Ali Kose**[3] | **Dilber Esra Yıldız**[4]

[1]Department of Electronics and Automation, Vocational High School, Bilecik Şeyh Edebali University, Bilecik, Turkey

[2]Department of Biotechnology, Faculty of Science, Selcuk University, Konya, Turkey

[3]Department of Chemistry, Faculty of Arts and Sciences, Hitit University, Corum, Turkey

[4]Department of Physics, Faculty of Arts and Sciences, Hitit University, Corum, Turkey

Correspondence
Adem Kocyigit, Department of Electronics and Automation, Vocational High School, Bilecik Şeyh Edebali University, Bilecik 11230, Turkey.
Email: adem.kocyigit@bilecik.edu.tr

Dilber Esra Yıldız, Department of Physics, Faculty of Arts and Sciences, Hitit University, Corum 19030, Turkey.
Email: desrayildiz@hitit.edu.tr

Cd and Co metal centered nicotinamide/nicotinic acid complexes were synthesized by chemical reactions. The complexes were characterized by thermogravimetric analysis (TGA), Fourier transform infrared spectroscopy (FT-IR), powder X-ray diffractometer (P-XRD), ultraviolet–visible (UV–Vis) spectrometer, and scanning electron microscopy (SEM) with energy dispersive X-ray (EDX) detector. The complexes were used as interfacial layers in between Al and p-Si to fabricate Al/Cd-complex/p-Si and Al/Co-complex/p-Si metal semiconductor devices. The devices were characterized by current–voltage (*I-V*) and current-time (*I-t*) measurements under dark and various light power intensities. The ideality factor, barrier height, and series resistance values were extracted from *I-V* measurements and discussed in detail by various techniques. The *I-t* measurements were used to derive various detector parameters such as responsivity, photosensitivity, and specific detectivity for various power values and wavelength regions. The devices exhibited good photodiode and photodetector performance according to results, and they can be improved for optoelectronic applications.

KEYWORDS

Al/p-Si, complex, metal semiconductor devices, nicotinamide/nicotinic acid, optoelectronic applications

1 | INTRODUCTION

The transition metals can be used with polymers to obtain complex structures for using in electronic and optoelectronic applications.[1–3] Especially, transition metal complexes have great attention owing to have good behaviors for various applications such as sensor technology, energy storage, and catalysis.[4–7] N or O atoms have been used to form two- or three-dimensional mesh structures when the molecules are composed as donor ligands. To support polymeric structure, the donor ligands are located as links between metal centers. Various ligands such as benzene-1,3,5-tricarboxylate, 1,2,4,5-benzenetetracarboxylate, dicarboxylate succinate, salicylates, terephthalate, and maleate can be used for binder in these structures.[8–14] These binding compounds are also named metal–organic frameworks (MOFs), and they have attracted great attention last decade due to having porosity as well as large surface areas that are important for separation and gas adsorption.[15–17] The porosity and surface area of the MOFs can easily be changed by various organic binders.[18–23] The chemical and structural behavior of coordination compounds can be adjusted by the same operation.[24–28]

Metal and semiconductor contacts are important for electronic devices because they can be ohmic or metallic contact at the same time depending on work function

differences of metal and semiconductor.[29–31] Sometimes an insulator or metal oxide interlayer can be inserted between metal and semiconductor to control charge conduction and stop leakage current or electrostatic charge generation.[32–35] Furthermore, this interfacial material can also increase effectivity of the metal–semiconductor contacts due to adjustable barrier height and passivate dangling bonds.[36–39] The synthesized MOFs or metal complexes can be used in the metal semiconductor contacts as an interfacial layer to obtain electronic devices.

In recent years, organic materials such as conjugated polymers and complex have attracted great interest in nanotechnology and nanoscience owing to easy and cost-effective method of developing organic materials and good properties for excellent flexible devices.[40,41] Organic materials have been commonly used for various device applications such as organic diode, photodiode, light-emitting display devices (LEDs), organic solar cells (OSCs), sensors, and supercapacitors.[42–49] Day by day developing technology and technological devices have increased the demand for inorganic materials in the world. This has led researchers to search for new alternative materials. Today, organic materials are considered by many researchers as an alternative to inorganic materials, and therefore, the investigation of device applications of these new materials has gained great importance in recent years. For instances, Cu(II) complex was used as interlayer between Al and p-Si and showed 2.7×10^{-3} A/W responsivity and 3.7×10^{8} Jones detectivity.[50] In another study, Ruthenium (III)–pyridine complex was used as an interlayer and showed excellent photodiode characteristics.[51] In our previous work, we investigated photodiode applications of complex materials. Co and Mn metal centered nicotinamide/nicotinic acid complexes were studied for photodetector applications and results revealed good detector performance.[52–54]

To enhance the electrical behaviors of MS devices in photodetector applications, the metal-complex structures can be used as an interfacial layer. Therefore, in this study, the Cd- and Co-complexes were synthesized chemically and employed as an interfacial layer for Al metal and p-Si semiconductor contact to obtain efficient photodiode or photodetector devices. Thus, Al/Cd-complex/p-Si and Al/Co-complex/p-Si devices were fabricated and tested under various light power intensities by *I-V* and *I-t* measurements.

2 | EXPERIMENTAL DETAILS

2.1 | Synthesis

Nicotinic acid ($C_6H_5NO_2$), N,N-diethylnicotinamide ($C_{10}H_{14}N_2O$), sodium bicarbonate ($NaHCO_3$), and cobalt acetate ($Co(CH_3COO)_2.4H_2O$) and cadmium acetate ($Cd(CH_3COO)_2.2H_2O$) were purchased from Sigma Aldrich. In order to increase the water solubility of nicotinic acid to be used for the synthesis of both metal complexes and facilitate its coordination, it was converted into its anionic form, its sodium salt (Scheme 1). For this purpose, 0.02 mol (2.462 g) nicotinic acid was taken into 50 ml distilled water, and 0.02 mol $NaHCO_3$ (1.68 g) was added to it. Natrium bicarbonate was added slowly to prevent overflow that may occur as a result of sudden CO_2 release. In the reaction sequence, 0.02 mol (3.565 g) N,N-diethylnicotinamide solution, which is the neutral ligand prepared in 50 ml of distilled water, was first added onto the anionic nicotinate ligand solution. In order to increase the homogeneity of the obtained solution, it was stirred for 30 min on a magnetic stirrer. Finally, acetate salts of the corresponding metal cations (for the Co(II) complex [0.01 mol and 2.491 g] and for the Cd(II) complex [0.01 mol (2.665 g)] to act as the coordination center of the complex) were slowly added to the individual reaction vessels as solids. Schemes 2 and 3 show the synthesis reaction scheme of Co(II) cation and Cd(II) cation centered nicotinic

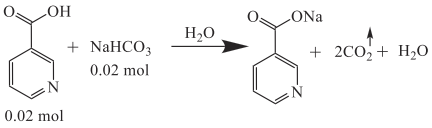

SCHEME 1 Synthesis reaction scheme of sodium salt nicotinicate

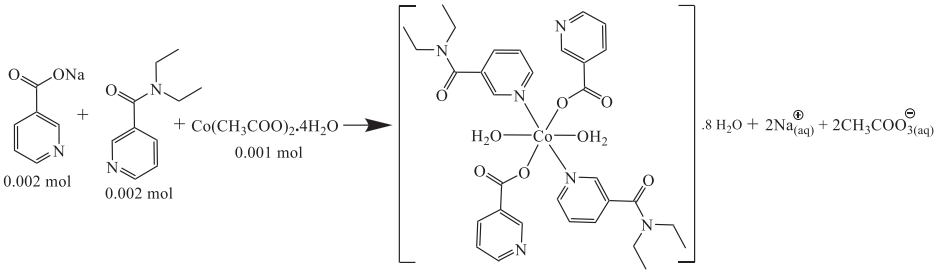

SCHEME 2 Synthesis reaction scheme of Co(II) cation centered nicotinic acid/N,N-diethylnicotinamide mixed ligand complex

SCHEME 3 Synthesis reaction scheme of Cd(II) cation centered nicotinic acid/N,N-diethylnicotinamide mixed ligand complex

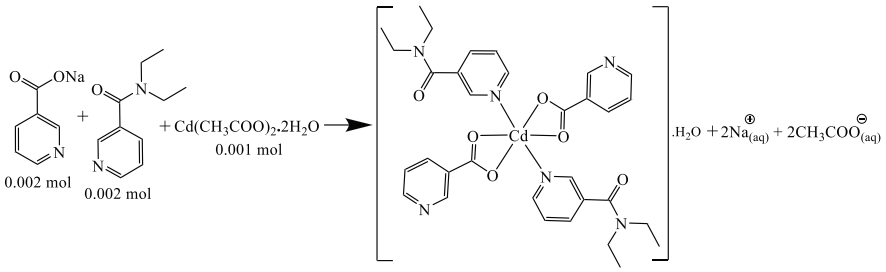

acid/N,N-diethylnicotinamide mixed ligand complex, respectively. The final total solution was stirred on a magnetic stirrer hot-plate at 60°C for 5 h.[25,55] The beaker in which it was transferred was covered with a perforated paraffin film and left to stand until crystal formation. After about 10–15 days, the respective metal cation complexes were allowed to aggregate as crystals of dark-pink for Co(II) and pale white for Cd(II) and stored for structural analysis.

2.2 | Device fabrications

p-Type Si wafer that had one-side polished surface was determined as semiconductor for fabricating photodiode or photodetector devices. The boron doped p-Si employed in this study had (100) crystalline orientation and 7.3×10^{15} cm^{-3} carrier concentrations. The wafer was sliced into 2×1 cm^2 pieces and cleaned in an ultrasonic cleaner by acetone, distilled water, and isopropanol for 30 min. HF:H_2O (1:10) solution was prepared to remove natural SiO_2 layers from surfaces of the p-Si wafer pieces for only 30 s. The pieces were transferred into a thermal evaporator to obtain 100 nm Al ohmic contact on the unpolished surfaces of the pieces and annealed at 450°C for 5 min in the N_2 filled oven. Then, the pieces were coated with the Cd- and Co-complex solution by a spin coating system for 30 s at 3000 rpm and dried softly at 80°C for 1 h. The coated pieces were again transferred into thermal evaporator to obtain metallic contacts on the Cd- and Co-complex surfaces by a hole array mask with 7.85×10^{-3} cm^2 area. Thus, Al/Cd-complex/p-Si and Al/Co-complex/p-Si devices were fabricated.

2.3 | Characterization

The Shimadzu TG60H instrument was employed for thermogravimetric analysis (TGA) analysis. The Shimadzu UV-3600i Plus ultraviolet–visible–near infrared (UV–vis–NIR) Spectrophotometer was used for UV–vis spectrometer measurements. Scanning electron microscopy (SEM) and energy dispersive X-ray (EDX) analysis were collected by ZEISS EVO LS 10 with @30 kV SE detector. Fytronix FY-7000 were employed to collect *I-V* and *I-t* measurements of the Al/Cd-complex/p-Si and Al/Co-complex/p-Si devices for dark and various light power illumination intensities. The response time was measured under the reverse bias of -2 V. A homemade light emitting diode (LED) system which had many LEDs with various wavelengths from visible to near infrared (NIR) was employed to illuminate devices.

3 | RESULTS AND DISCUSSION

3.1 | Structural properties

Chemical composition analysis data for the molecule confirm the proposed molecule formula. For the Co(II) complex, experimental, C:46.07%; H:6.99%; N:10.07%, calculated, C:45.77%; H:6.72%; N:10.01%. For the Cd(II) complex, experimental, C:51.98%; H:5.72%; N:11.43%, calculated, C:52.57%; H:5.24%; N:11.50%. The thermal analysis curves showing the decomposition steps and decomposition products of the complexes of Co(II) and Cd(II) metals with nicotinic acid/N,N-diethylnicotinamide ligands are shown in Figure 1. Also, the data obtained from the curves are listed in Table 1. Depending on the different structures of Co(II) and Cd(II) metal complexes, thermal decomposition steps also show differences (Figure 1). It is suggested that the nicotinate (*na*) and N,N-diethylnicotinamide (*dena*) ligands present in the Co(II) structure show monodentate bonding and the structure makes the coordination of the metal with the two aqua ligands in the coordination sphere hexagonal. It is claimed that the thermal degradation curve of the Co(II) structure belongs to the removal of 10 aqua molecules in the range of 73–222°C and that two of these aqua molecules are waters in coordination, and the other eight hydrate waters are located outside the coordination sphere and attached to the structure by hydrogen bonds. The agreement of the theoretical and experimental weight losses also supports the claim (den. 21.22%; theo. 21.45%). The next decomposition step, which takes place endothermically in the temperature

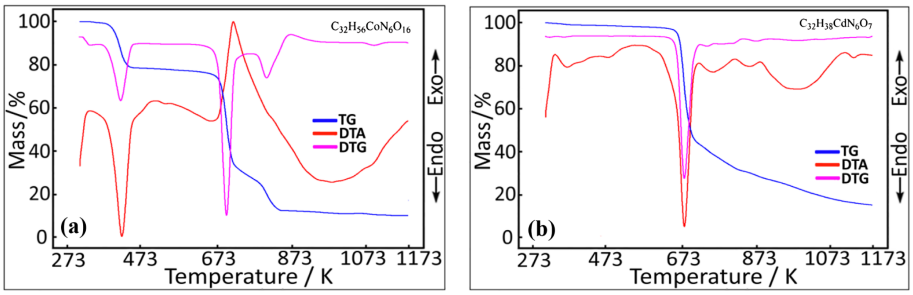

FIGURE 1 Thermogravimetry-derivative thermogravimetry (TG-DTG) and differential thermal analysis (DTA) curves of the $[Ni(C_6H_4NO_2)_2(C_{10}H_{14}N_2O)_2(H_2O)_2]\cdot 7H_2O$ (a) and $[Zn(C_6H_4NO_2)_2(C_{10}H_{14}N_2O)_2]\cdot H_2O$ (b) complexes

TABLE 1 Thermal analysis data of metal-nicotinate/N,N-diethylnicotinamide mixed ligand complex

Complexes		Temp. Range (°C)	DTA_{max} (°C)	Removed Groups	Mass Loss (%)		Remain Product (%)		Decomp. product	Color
					Exp.	Calc.	Exp.	Calc.		
$[Co(C_6H_4NO_2)_2(C_{10}H_{14}N_2O)_2(H_2O)_2]\cdot 8H_2O$										Dark-pink
$C_{32}H_{56}CoN_6O_{16}$	1	73–222	134	10 H_2O	21.22	21.45				
839.76 g/mol	2	343–441	−430	2 $C_{10}H_{14}N_2O$	42.81	42.45				
	3	443–777	695	$C_6H_4NO_2$ C_6H_4NO	25.89	27.17	10.08	8.92	CoO	Black
$[Cd(C_6H_4NO_2)_2(C_{10}H_{14}N_2O)_2]\cdot H_2O$										White
$C_{32}H_{38}N_6O_7Zn$	1	53–300	90;200	H_2O	2.29	2.46				
684.07 g/mol	2	336–421	401	2 $C_{10}H_{14}N_2O$	49.12	48.76				
	3	425–856	480;573;700	$C_6H_4NO_2$ C_6H_4NO	30.30	31.21	18.29	17.14	CdO	Black

range of 343–441°C, can be attributed to the combustion of two *dena* ligands, which provide neutral coordination to the structure through the pyridine nitrogen (den. 42.81%; theo. 42.45%). The last decomposition step is the thermal decomposition step, in which the remaining organic residues (monoanionic coordinated *na* ligand over acidic oxygens) are decomposed by combustion (den. 25.89%; theo. 27.17%). It was confirmed by powder X-ray diffraction (XRD) analysis (data not shown here) that CoO residue remained in the reaction vessel as a result of thermal decomposition, and the compatibility of experimental and theoretical weight losses also supports this claim.

The thermal decomposition of the metal cation-centered structure of the other metal complex, Zn(II), also begins with dehydration. Since the d^{10} structure and radius of the Cd(II) metal cation are larger than the Co(II) cation, it is thought that the nicotinic acid ligand binds to the Cd(II) metal monoanionic-bindentically on two oxygens (acidic and carbonyl oxygens). The coordination of the metal with two bidentate-bound *na* ligands and two monodentate-bound *dena* ligands in the coordination sphere completes the hexagonal. Therefore, it does not contain any aqua ligand in its coordination sphere. The dehydration we have mentioned is attributed to the removal of one hydrated water located outside the coordination sphere (den. 2.29%; theo. 2.46%). The thermal degradation steps, which are attributed to the combustion of organic ligands in the structure after the dehydration step, are very similar to the Co(II) complex structure. It is thought that it consists of the burning of two *dena* ligands first and then the combustion of two *na* ligands, which are coordinated to bidentate in the structure. It is thought that CdO residue remains as the final residual product of thermal degradation. It has been observed that the experimental and theoretical weight losses, which can be shown as support for these claims, are compatible (Table 1).

It has been determined that the experimental weight losses of the relevant metal oxide residues remaining as a result of the thermal decomposition of both complexes are approximately 1.5% higher than the theoretical weight losses. It is thought that the reason for this mismatch is that the structures do not have enough oxygen source to burn all the carbon residues in the thermal decompositions carried out in inert nitrogen atmosphere, and therefore, due to insufficient oxygen, some non-combustible carbon residues are deposited on the surface

of the metal oxides in the form of carbonized carbon. The fact that the color of both metal oxide residues is black also supports this claim.[56]

Fourier transform infrared spectroscopy (FT-IR) technique was employed to illuminate molecular structure of the Co(II)- and Cd(II)-complexes. Significant stretching vibrations of Cd(II) and Co(II) metal cation complexes have been shown in Figure 2 and Table 2 in the range of 4000–400 cm^{-1} by FT-IR spectroscopy technique. The absence of hydrate molecules in the structure of the Cd(II) complex was also confirmed by the infrared spectrum. A corresponding peak was not observed in the region of 3600–3000 cm^{-1}, which could be attributed to the –OH groups of the hydrate ligand and was expected to appear as a strong and broad peak. In the Co(II) complex, which is claimed to coordinate two aqua ligands to the metal cation in its structure, a strong and broad peak is observed in the 3600–3000 cm^{-1} region due to the –OH groups. Strong and sharp peaks seen at 3473 cm^{-1} in the Cd(II) structure and 3355 cm^{-1} in the Co(II) structure can be interpreted to the amide group of the N,N-diethylnicotinamide ligand in both structures. The 2960–2850 cm^{-1} peaks detected in both structures belong to the aliphatic ethylene chains attached to the amide group (somewhat screened by the strong and broad –OH peak in the Co(II) complex). The carbonyl ν(C=O) stretch of the carboxylate group, which appeared in the 1750 cm^{-1} region of the uncoordinated nicotinate ligand, shifted to the right in both complexes and peaked at 1656 cm^{-1} in the Cd(II) structure and 1683 cm^{-1} in the Co(II) structure. It can be said that the binding of the ν(C=O) group shifted to a lower region compared to the Co(II) complex (1683 cm^{-1}), due to the fact that the carboxylate group binds both from acidic oxygen and carbonyl oxygen to bidentate in the Cd(II) complex. The difference between the symmetrical and asymmetrical stretches of the carboxylate group should be avoided as evidence of the monoanionic-bidentate binding of the nicotinate ligand from the carboxylate group in the Cd(II) complex, while the monoanionic-monodentate binding in the Co(II) complex. The difference between the symmetrical and asymmetric tension vibrations of the carboxylate group in the monoanionic-monodentate-linked sodium salt structure of the nicotinate molecule is 155 cm^{-1}. Coordination with a value greater than this difference is considered to bind to bidentate, and if it is less than or equal to this value, it is considered to bind to monodentate. In the Cd(II) structure, the symmetrical stretching vibration of the $\nu(COO^{-})$ group was found to be 1604 cm^{-1}, and the asymmetric stretching vibration was found to be 1401 cm^{-1}. The difference between the two values was calculated as 203 cm^{-1}, which indicates the binding of the nicotinate ligand from the carboxylate group to bidentate. In the Co(II) complex, on the other hand, the symmetrical stretching vibration of the $\nu(COO^{-})$ group is 1535 cm^{-1}, and the asymmetrical stretching vibration is 1397 cm^{-1}, and the difference between them is calculated as 138 cm^{-1}. This difference indicates that the nicotinate ligand binds to the Co(II) metal cation, monoanionic-monodentate.[57] In the fingerprint regions of the infrared spectra of both complexes, it was observed that the stretch vibrations of the related binding of nicotinate and N,N-diethylnicotinamide ligands in the structures appeared in

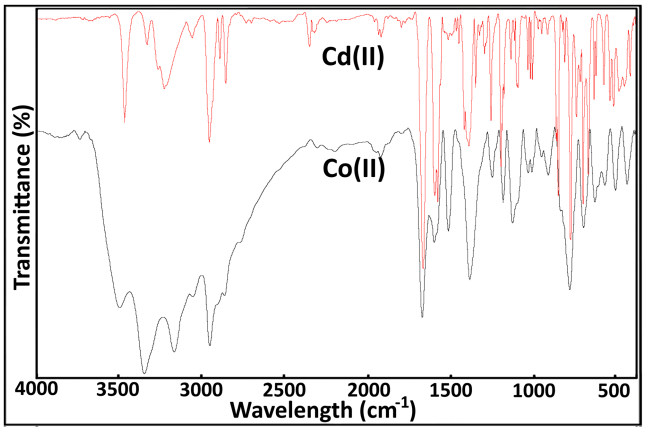

FIGURE 2 Fourier transform infrared spectroscopy (FT-IR) spectra of Cd(II) and Co(II) coordination compounds

TABLE 2 Some important FT-IR peaks of Cd(II) and Co(II) complexes

Gruplar	Cd(II)	Co(II)
$\nu(OH)_{H2O}$	-	3680–3000
$\nu(=C–H)_{aromatic}$	3235	3175
$\nu(CH_3)_{aliphatic}$	2963	2961
$\nu(CH_2)_{aliphatic}$	2900,2865	2906,2848
ν(C=O)	1676	1683
$\nu(C=C)_{arom.}$	1614	1610
$\nu(COO–)_{asym.}$	1604	1535
$\nu(COO–)_{sym.}$	1401	1397
$\Delta\nu_{asym\text{-}sym}$	203	138
$\nu(C–N–C)_{pyridin}$	1359	1355
$\nu(C_9–O_1–C_1)$	1269/1190	1262/1196
ν(Ring)	1105–787	1139–795
$\nu(C–N)_{amid}$	873–730	845–712
ν(M–N)	635	644
$\nu(M–O–)_{carboxyl}$	528	521
$\nu(M–O=)_{carbonyl}$	496	-
$\nu(M–O–)_{aqua}$	-	450

similar regions, although there were very small differences (Table 2). The ν(M-N) binding of ligands indicating their coordination to metal cations was observed at 635 cm^{-1} for the Cd(II) complex, whereas it was observed in the 644 cm^{-1} region for the Co(II) complex. Peaks indicating the coordination of carboxylic acid oxygen common to both structures were determined as 528 cm^{-1} for Cd(II) structure and 521 cm^{-1} for Co(II) structure. While the peak indicating the coordination of the carbonyl group oxygen occurring in the Cd(II) complex was observed at 496 cm^{-1}, the relevant peak could not be observed in the Co(II) structure. When the peak indicating the binding of the two coordination waters present in the Co(II) complex was detected at 450 cm^{-1}, this peak was absent in the Cd(II) complex that did not contain the hydrate ligand.[26,58]

Powder X-ray diffraction (P-XRD) patterns were recorded in the two theta axes of both complex structures. Figure 3 exhibits P-XRD patterns of the Cd(II) and Co(II) complexes. It can be said that the crystallinity of the structures is not very high. The louder observed P-XRD pattern of the Cd(II) complex shows that the structure is more amorphous compared with Co(II) complex. It can be claimed that the Co(II) complex, which contains two hydrate ligands in its structure, increases the crystallinity with the intramolecular hydrogen bonds formed by these hydrate waters. The sharp and high-intensity distinct peaks among the noisy peaks observed in the patterns belong to the related metal complex structures. The differences in the two theta regions of the peaks appearing in the P-XRD patterns were observed due to the differences in metal cations in the structures of the complexes and the coordination differences present in the structures.

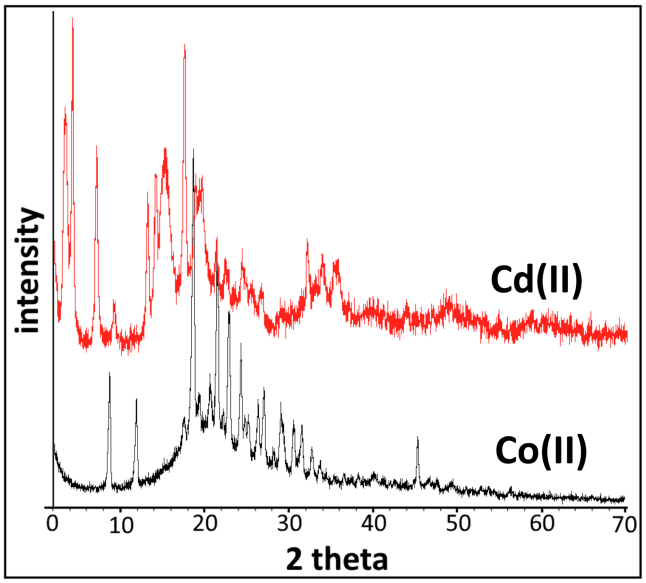

FIGURE 3 Powder X-ray diffractometer (P-XRD) patterns of Cd(II) and Co(II) complexes

The UV–vis spectrometer was used to obtain band gap (E_g) curves. Figure 4a,b exhibits E_g curves of the Co(II) and Cd(II) complexes, respectively. While the Co(II) complex has band gap value of 3.84 eV, the Cd(II) complex has 3.99 eV. These values are extremely high for solar cell devices, but the complexes can be used for UV photodetector devices.

3.2 | Morphological properties

Morphological behaviors of the Co(II) and Cd(II) complexes were studied by SEM and fast map EDX analysis. Figure 5a,b displays SEM–EDX fast map analysis and EDX spectrum of the Co(II) and Cd(II) complexes, respectively, for wide range surface area. The Co(II) and Cd(II) complexes have uniform surface area and smooth surfaces. Both samples have silicon due to substrate, carbon, nitrogen, and oxygen atoms homogeneously. Whereas Co(II) complex has cobalt atoms, Cd(II) complex has cadmium atoms. The EDX spectrums of the Co(II) and Cd(II) complexes also clearly indicate peaks of these atoms. The result clearly

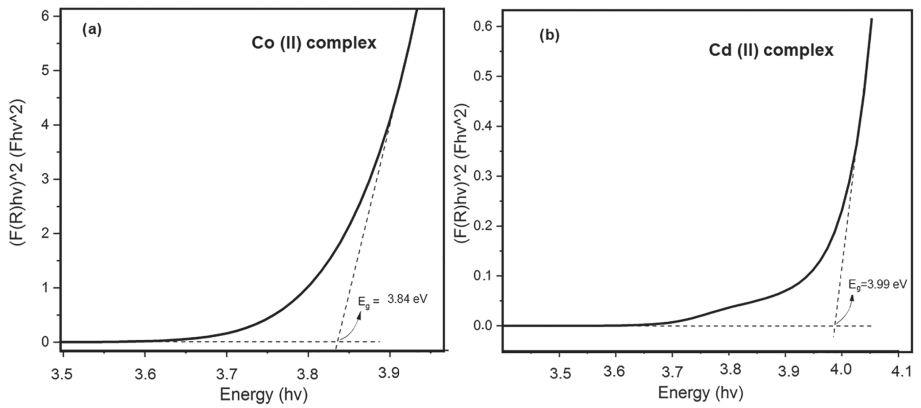

FIGURE 4 E_g curves of (a) Co(II) complex and (b) Cd(II) complex

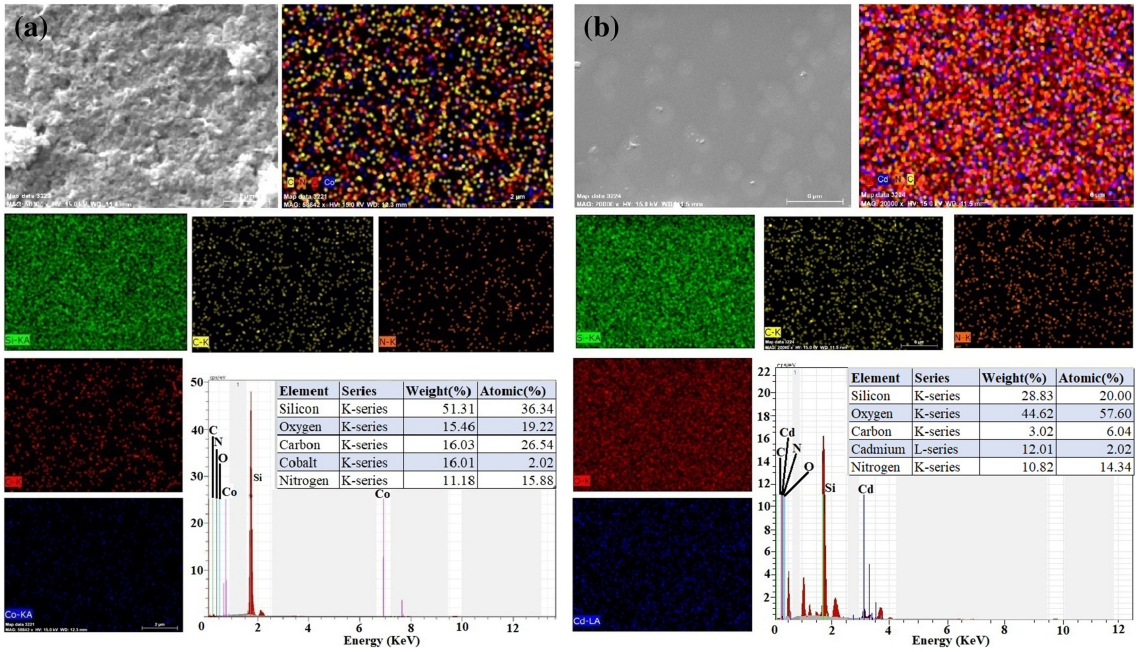

FIGURE 5 Scanning electron microscopy–energy dispersive X-ray (SEM–EDX) fast map analysis of (a) Co(II) complex and (b) Cd(II) complex

FIGURE 6 ln*I-V* plots of the (a) Al/Cd-complex/p-Si and (b) Al/Co-complex/p-Si devices for various illumination conditions

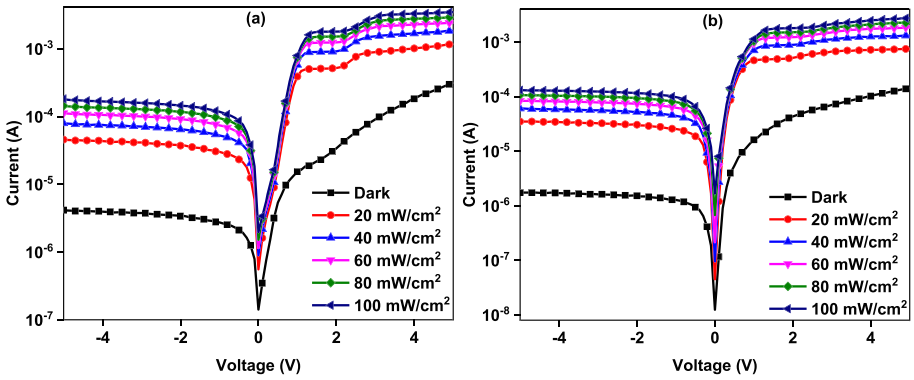

confirmed the chemical composition and good morphology of the Co(II) and Cd(II) complexes.

3.3 | Electrical properties

Electrical characteristics of the Al/Cd-complex/p-Si and Al/Co-complex/p-Si devices have been investigated under dark as well as under various illumination intensities by *I-V* measurements. ln*I-V* plots of the Al/Cd-complex/p-Si and Al/Co-complex/p-Si devices have been displayed in Figure 6a,b, respectively, for changing light power from dark to 100 mW/cm^2. Both devices exhibited good increase at the photocurrent at reverse and forward biases. The devices can be thought of for photodetector and photodiode applications due to having light induced currents for increasing light power intensity.[59,60] The current values are higher at forward biases than reverse biases even if light illumination conditions. Thus, the devices can be employed in photodiode applications.

Rectification ratio (*RR*) value reveals the diode efficiency for conducting the current at forward biases and stopping at reverse biases.[61] Figure 7a,b exhibits the *RR* value changes of the Al/Cd-complex/p-Si and Al/Co-complex/p-Si devices, respectively at ±3 V. Both devices showed low *RR* values, and they decreased with increasing light power owing to increasing current with increasing light power.

The barrier height (Φ_b) and ideality factor (n) values of devices can be determined by thermionic emission theory to understand the structure of the fabricated devices. While the n value exhibits a diode close to the ideal

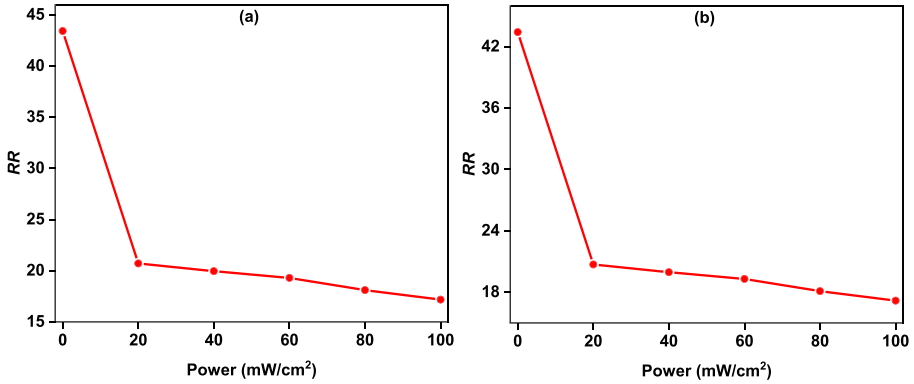

FIGURE 7 Rectification ratio (*RR*) profiles of the (a) Al/Cd-complex/p-Si and (b) Al/Co-complex/p-Si devices for changing light power intensity

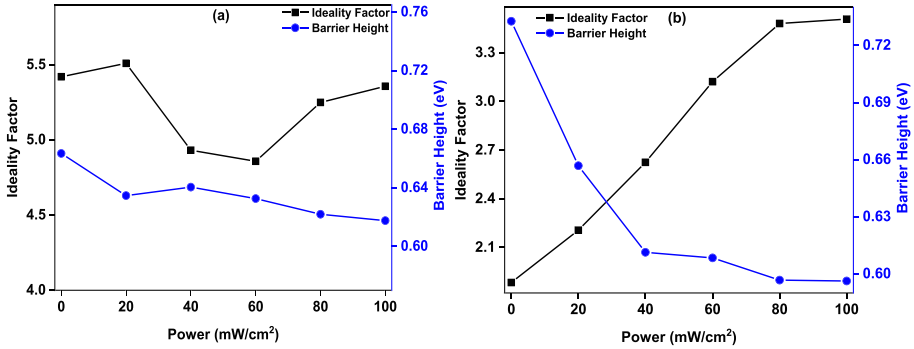

FIGURE 8 n-Φ_b plots of the (a) Al/Cd-complex/p-Si and (b) Al/Co-complex/p-Si devices for changing light power intensity

TABLE 3 The device parameters of the Al/Cd-complex/p-Si and Al/Co-complex/p-Si devices

Device Interlayer	Saturation Current (A)	n (I-V) -	n Cheung -	Φ_b (I-V) (eV)	Φ_b Cheung (eV)	Φ_b Norde (eV)	R_s Cheung (kΩ ($H(I)$))	R_s Cheung (kΩ ($d\ln(I)$))	R_s Norde (kΩ)
Cd-complex	1.66×10^{-7}	5.42	5.48	0.66	0.70	0.69	17.16	17.18	4.73
Co-complex	1.14×10^{-8}	1.88	1.74	0.73	0.77	0.78	36.64	36.59	10.49

condition, barrier height shows the degree of the barrier in the junction. Figure 8a,b displays the ideality factor and barrier height changes of the Al/Cd-complex/p-Si and Al/Co-complex/p-Si devices depending on the increasing light power intensity. While the barrier height values decreased with increasing light power intensity, the ideality factor values increased for Al/Co-complex/p-Si device and slightly changed for the changing light power. The higher ideality factor values than unity can be ascribed to interfacial layer as well as interface states.[62] The calculated n and Φ_b values have been listed in Table 3 for the Al/Cd-complex/p-Si and Al/Co-complex/p-Si devices in dark condition.

The junction resistance (R_j) of the metal semiconductor devices helps to know series (R_s) and shunt (R_{sh}) resistances and is obtained from I-V characteristics by the formula of $R_j = dV/dI$.[63] While the forward bias region exhibits R_s, reverse bias region shows R_{sh}. Generally, the high R_{sh} and low R_s values are desired for a good performance device. The R_j versus voltage plots of the Al/Cd-complex/p-Si and Al/Co-complex/p-Si devices have been illustrated in Figure 9a,b, respectively. The R_{sh} values of the Al/Cd-complex/p-Si and Al/Co-complex/p-Si devices were obtained about 10^6 Ω level, and R_s values were obtained as around 10^4 Ω level. The R_s values are high for both devices and can be decreased by decreasing errors as well as healing of experimental setup.

Norde technique is another technique to calculate barrier height as well as series resistance values by using Norde function, which was obtained by Norde.[64] Figure 10a,b indicates Norde function plots of the Al/Cd-complex/p-Si and Al/Co-complex/p-Si devices, respectively. The devices exhibited normal Norde function plot, and the barrier height and series resistance values were calculated. The results have been given in Table 3 for Al/Cd-complex/p-Si and Al/Co-complex/p-Si devices. The obtained Φ_b values are slightly higher than the Φ_b values, which were obtained from thermionic emission

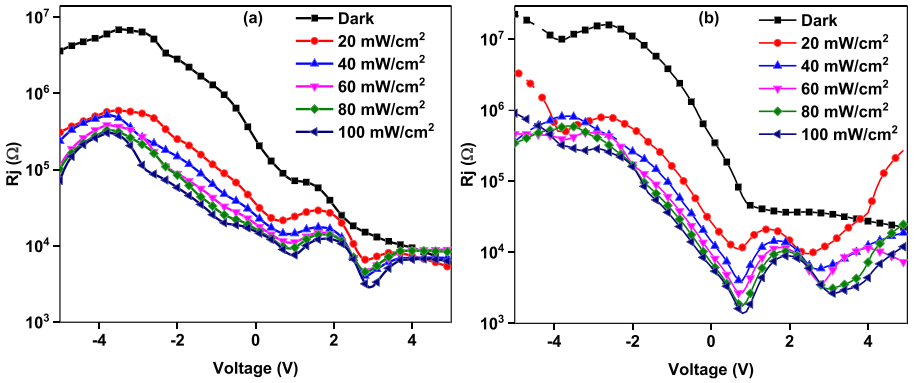

FIGURE 9 R_j-V plots of the (a) Al/Cd-complex/p-Si and (b) Al/Co-complex/p-Si devices for changing light power intensity

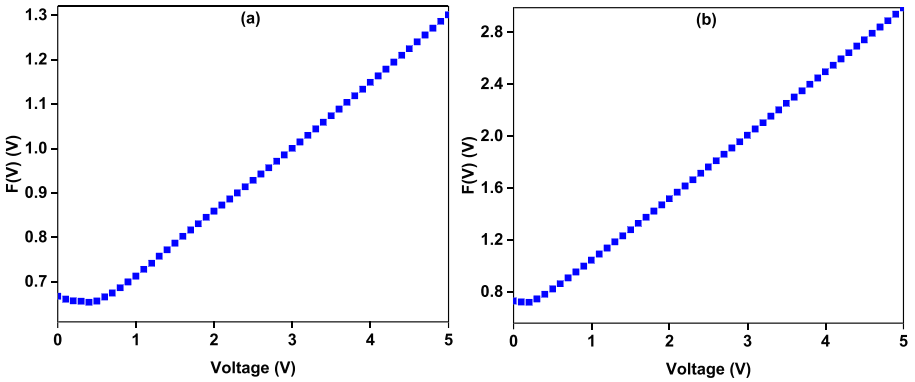

FIGURE 10 Norde fuction plots of the (a) Al/Cd-complex/p-Si and (b) Al/Co-complex/p-Si devices for changing light power intensity

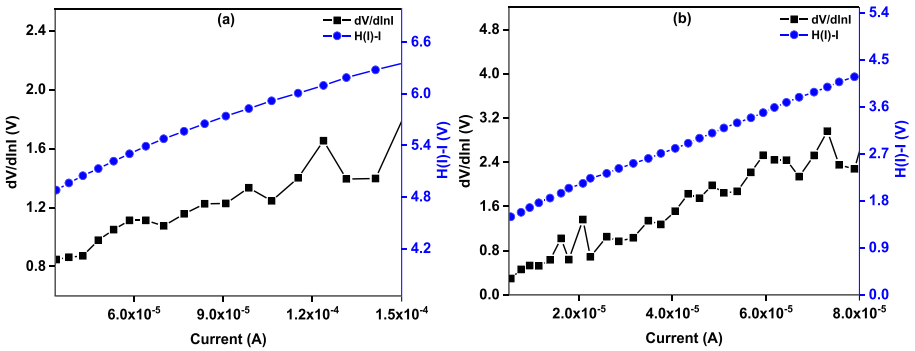

FIGURE 11 Cheung plots of the (a) Al/Cd-complex/p-Si and (b) Al/Co-complex/p-Si devices for changing light power intensity

theory for both devices owing to approximation differences.[65]

The Cheung is also another technique to calculate barrier height, ideality factor, and series resistance values for these kinds of devices. The technique uses Cheung functions ($dV/d\ln(I)$ and $H(I)$) plots depending on the current.[31,66] While the y-intercept of the $dV/d\ln(I)$ function helps to calculate n value, $H(I)$ function provides to determine Φ_b. The slopes of both functions give to different series resistances, which have to close each other for consistency of the Cheung technique. Figure 11a,b shows Cheung plots of the Al/Cd-complex/p-Si and Al/Co-complex/p-Si devices, and calculated n, Φ_b, and series resistance values have been listed in Table 3. The calculated values have some discrepancies calculated from other techniques due to non-ideal device structure as well as interfacial layer effect.

The photocurrent transient or current on–off measurements are used to determine photoconducting and photoresponse mechanism of the optoelectronic devices. Thus, responsivity, photosensitivity, and detectivity characteristics can be obtained depending on the changing power intensity.[67–70] Figure 12a,b reveals photocurrent transient measurements of the Al/Cd-complex/p-Si and Al/Co-complex/p-Si devices for increasing light power intensity from 20 to 100 mW/cm^2, respectively. Both devices exhibited almost linearly increase with increasing light power.

The detector parameters of the Al/Cd-complex/p-Si and Al/Co-Complex/p-Si devices were calculated by

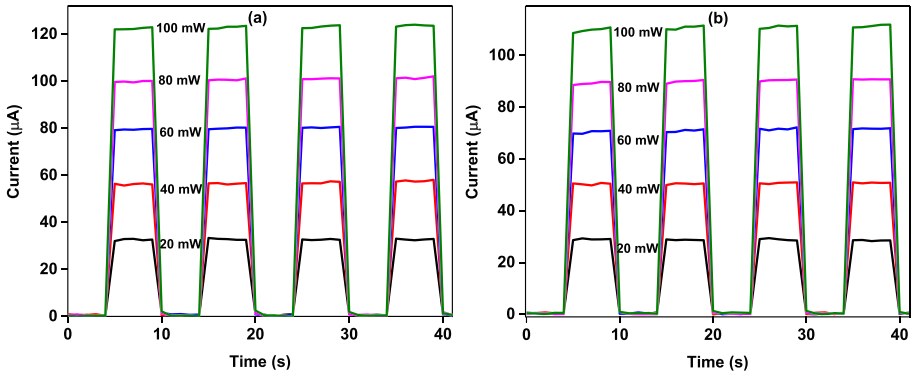

FIGURE 12 *I-t* plots of the (a) Al/Cd-complex/p-Si and (b) Al/Co-complex/p-Si devices for changing light power intensity

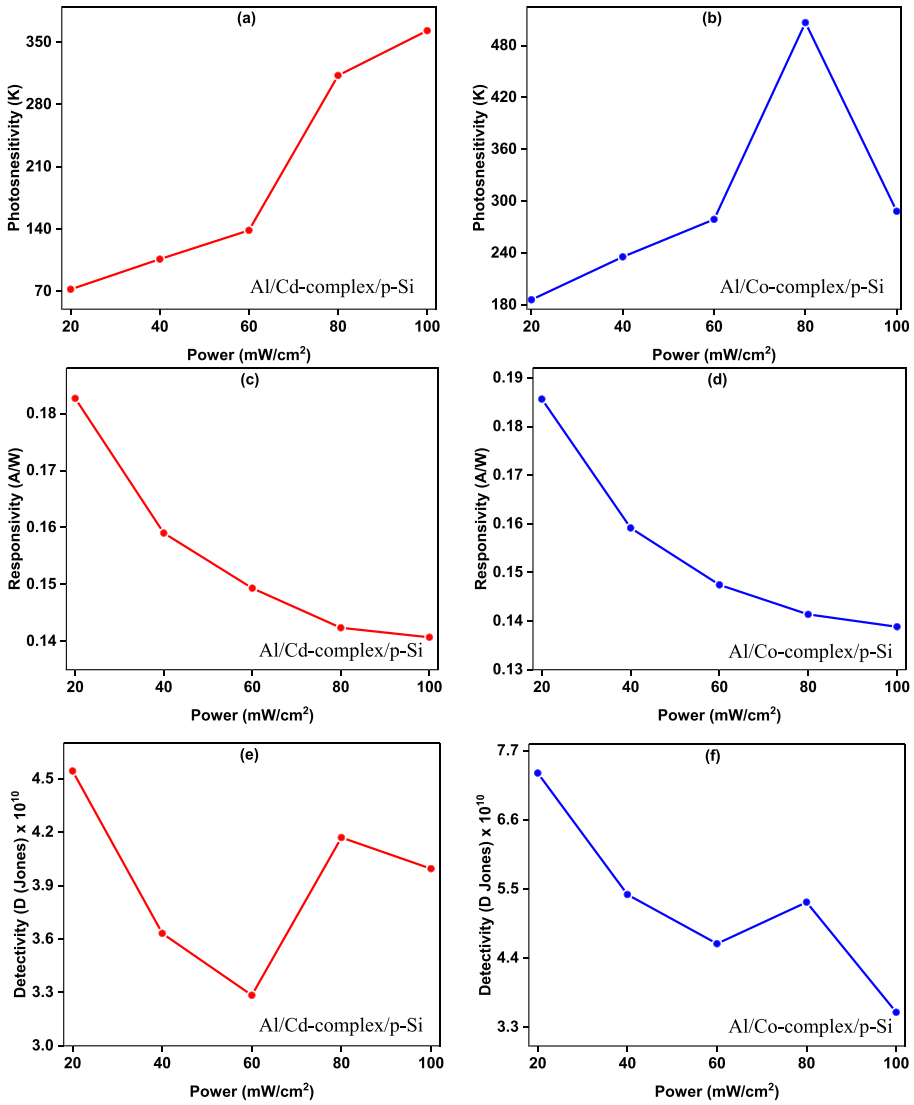

FIGURE 13 (a,b) Photosensitivity, (c,d) responsivity, and (e,f) detectivity profiles of the Al/Cd-complex/p-Si and Al/Co-complex/p-Si devices depending on creasing light power intensity

using of the current transient measurements. The photocurrent (I_p), photosensitivity (K), responsivity (R), and specific detectivity (D^*) equations are given by following formula, respectively.

$$I_p = I_{light} - I_{dark}, \quad (1)$$

$$K = \frac{I_p}{I_{dark}}, \quad (2)$$

$$R = \frac{I_p}{PA}, \tag{3}$$

$$D^* = R\sqrt{\frac{A}{2qI_{dark}}}, \tag{4}$$

$$EQE = R\frac{hc}{q\lambda_{nm}}, \tag{5}$$

where P exhibits incident power density and A is detector area. The h, c, and λ_{nm} show Planck constant, speed of light, and wavelength of incident light in nm, respectively.

Figure 13a,b shows photosensitivity versus light power intensity profiles of the Al/Cd-complex/p-Si and Al/Co-Complex/p-Si devices, respectively. While the device almost has linear change with increasing light power, the Al/Co-Complex/p-Si device has some discrepancy from linearity for 100 mW/cm^2 light power illumination intensity. Both devices have pretty high photoresponsivity with illumination. Figure 13c,d displays responsivity changes of the Al/Cd-complex/p-Si and Al/Co-Complex/p-Si devices, respectively, for increasing light power. The devices have good responsivity values, and their values slightly decreased with increasing light power intensity. These results are compatible with current literature for Schottky type photodiodes or photodetectors.[71,72] Figure 13e,f indicates specific detectivity profiles of the Al/Cd-complex/p-Si and Al/Co-Complex/p-Si devices, respectively, for changing light power intensity. The D^* values decreased towards 60 mW/cm^2 light power intensity and then increased for 80 mW/cm^2 light power intensity and again decreased slightly for 100 mW/cm^2 light power intensity. The obtained D^* values are 10^{10} Jones level, and they are good harmony for a kind of Schottky type photodetector devices.[73]

Responsivity and external quantum efficiency (EQE) values were studied by homemade LED system, which had illuminations at various wavelengths. However, every LED has different power illumination density according to pyranometer measurements. Inset of Figure 14a shows power of the LEDs depending on the wavelengths. The responsivity wavelength profiles of the Al/Cd-complex/p-Si and Al/Co-complex/p-Si devices have been illustrated in Figure 14a,b, respectively. Both devices have exhibited response almost entire visible and NIR regions. However, their responsivity values are low due to Schottky structure.[74,75]

The EQE value represents how many electrons are provided to the external circuit for each photon that strikes the device.[76] The primary physical factor affecting photocarrier collecting efficiency is called EQE. It is also crucial for the practical use of optoelectronic devices.[77] Figure 14c,d indicates EQE profiles of the Al/Cd-complex/p-Si and Al/Co-complex/p-Si devices, respectively, for various wavelengths. The devices have high EQE values than 100% due to the fact that one

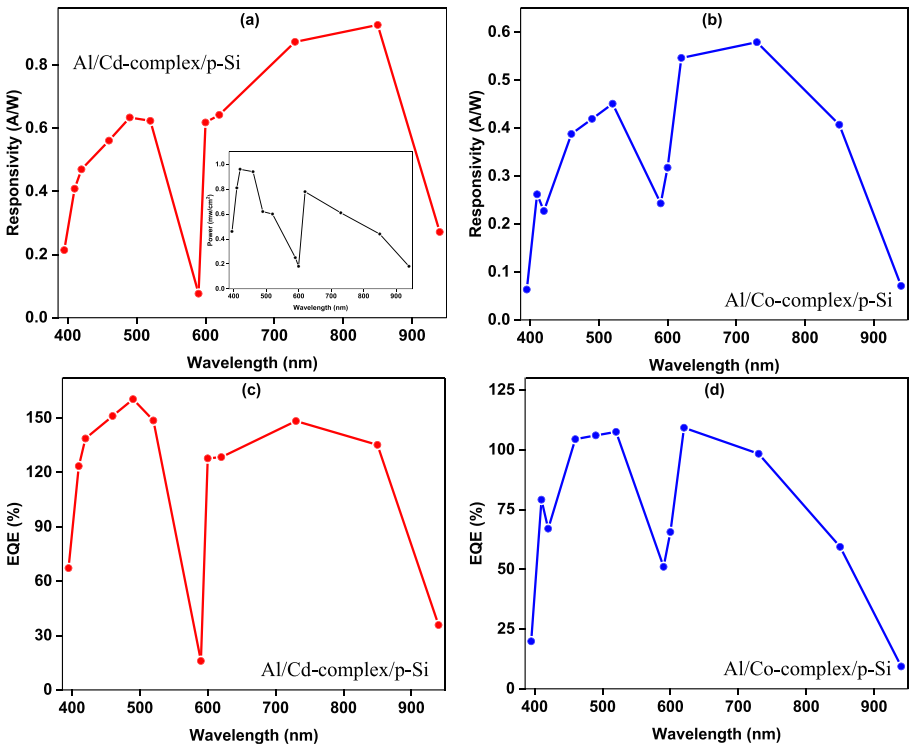

FIGURE 14 (a,b) Responsivity and (c,d) external quantum efficiency (EQE) profiles of the Al/Cd-complex/p-Si and Al/Co-complex/p-Si devices for changing wavelength

photon might be excited more than one electron or tunneling of the barrier by carriers in the interface of Schottky photodiodes.[78] The devices almost have high EQE values for entire visible and NIR region of the spectrum. Results confirm that the devices can be employed as photodetector visible and NIR regions.

4 | CONCLUSION

Nicotinamide/nicotinic acid complexes with centered of Cd and Co metal were synthesized by chemically and used as interfacial layer in between Al and p-Si to fabricate Al/Cd-complex/p-Si and Al/Co-complex/p-Si metal semiconductor devices. The TGA analysis confirmed clearly the composition of the Co- and Cd complexes. The FT-IR spectroscopy results revealed molecular vibration of the complex structures. The P-XRD approved crystalline structure of metal complexes. The UV–vis spectrometer results revealed that band gaps of the Co-complex and Cd-complex were 3.84 and 3.99 eV, respectively. The SEM and EDX analyses revealed that the Co-complex and Cd-complexes exhibited uniform surface and good atomic distribution. The devices were characterized by *I-V* and *I-t* measurements under dark and various light power intensities. While the ideality factor values of the Al/Cd-complex/p-Si and Al/Co-complex/p-Si devices were calculated as 5.42 and 1.88, respectively, barrier height values were obtained as 0.66 and 0.73 eV from thermionic emission theory. The Norde and Cheung techniques also were employed to confirm these parameters as well as to depict series resistance values. The *I-t* measurements were used to derive various detector parameters such as responsivity, photosensitivity, and specific detectivity. The obtained detector parameters are good enough for a kind of photodetector. The devices exhibited good photodiode and photodetector performance according to results for visible and NIR regions, and they can be improved for optoelectronic applications.

CONFLICT OF INTEREST

The authors declare that they have no conflict of interest.

AUTHOR CONTRIBUTIONS

Adem Kocyigit: Conceptualization; visualization. **Ali Akbar Hussaini:** Data curation; methodology. **MURAT YILDIRIM:** Data curation; methodology; visualization. **Dursun Ali Köse:** Data curation; methodology; visualization. **Dilber Esra Yıldız:** Investigation; supervision; visualization.

DATA AVAILABILITY STATEMENT

Data is available upon reasonable requests.

ORCID

Adem Kocyigit https://orcid.org/0000-0002-8502-2860
Ali Akbar Hussaini https://orcid.org/0000-0002-7128-9994
Murat Yıldırım https://orcid.org/0000-0002-4541-3752
Dursun Ali Kose https://orcid.org/0000-0003-4767-6799
Dilber Esra Yıldız https://orcid.org/0000-0003-2212-199X

REFERENCES

[1] N. Sari, E. Kahraman, B. Sari, A. Özgün, *J. Macromol. Sci. Part A Pure Appl. Chem.* **2006**, *43*, 1227.
[2] Z. S. Şahin, M. Demir, T. Yıldırım, Ö. Yurdakul, D. A. Köse, *Int. J. Hydrogen Energy* **2021**, *46*, 27631.
[3] Ö. Yurdakul, Z. S. Şahin, D. A. Köse, O. Şahin, F. Akkurt, *J. Mol. Struct.* **2020**, *1218*, 128514.
[4] C. N. R. Rao, S. Natarajan, R. Vaidhyanathan, *Angew. Chem. Int. Ed.* **2004**, *43*, 1466.
[5] J. Kim, U. Lee, B. K. Koo, *Bull. Korean Chem. Soc.* **2010**, *31*, 487.
[6] O. V. Nesterova, A. J. L. Pombeiro, D. S. Nesterov, *Materials (Basel).* **2020**, *13*, 1.
[7] M. S. A. Abdel-Mottaleb, E. H. Ismail, *J. Chem.* **2019**, *2019*. https://doi.org/10.1155/2019/3241061
[8] J. Kim, U. Lee, B. K. Koo, *Bull. Korean Chem. Soc.* **2010**, *31*, 1743.
[9] B. K. Koo, J. Kim, U. Lee, *Inorg. Chim. Acta* **2010**, *363*, 1760.
[10] Y. B. Go, X. Wang, E. V. Anokhina, A. J. Jacobson, **Inorg. Chem.* **2005**, *44*, 8265.
[11] H. Xu, R. Wang, Y. Li, *J. Mol. Struct.* **2004**, *688*, 1.
[12] N. Hao, Y. Li, E. Wang, E. Shen, C. Hu, L. Xu, *J. Mol. Struct.* **2004**, *697*, 1.
[13] B. K. Koo, *Bull. Korean Chem. Soc.* **2012**, *33*, 2299.
[14] O. M. Yaghi, H. Li, C. Davis, D. Richardson, T. L. Groy, *Acc. Chem. Res.* **1998**, *31*, 474.
[15] Z. Zhang, Y. Zhao, Q. Gong, Z. Lib, J. Li, *Chem. Commun.* **2013**, *49*, 653.
[16] A. E. Baumann, D. A. Burns, B. Liu, V. S. Thoi, *Commun. Chem.* **2019**, *2*, 1.
[17] A. A. García-Valdivia, S. Pérez-Yáñez, J. A. García, B. Fernández, J. Cepeda, A. Rodríguez-Diéguez, *Sci. Rep.* **2020**, *10*, 1.
[18] H. K. Chae, J. Kim, O. D. Friedrichs, M. O'Keeffe, O. M. Yaghi, *Angew. Chem. Int. Ed.* **2003**, *42*, 3907.
[19] H. C. Zhou, J. R. Long, O. M. Yaghi, *Chem. Rev.* **2012**, *112*, 673.
[20] U. Mueller, M. Schubert, F. Teich, H. Puetter, K. Schierle-Arndt, J. Pastré, *J. Mater. Chem.* **2006**, *16*, 626.
[21] M. Jacoby, *Chem. Eng. News* **2008**, *86*, 13.
[22] M. Eddaoudi, J. Kim, N. Rosi, D. Vodak, J. Wachter, M. O'Keeffe, O. M. Yaghi, *Science (80-.)* **2002**, *295*, 469.
[23] Z. Wang, S. M. Cohen, *J. Am. Chem. Soc.* **2007**, *129*, 12368.
[24] D. A. Köse, B. Öztürk, O. Şahin, O. Büyükgüngör, *J. Therm. Anal. Calorim.* **2013**, *115*, 1515.
[25] D. A. Köse, F. Akkurt, O. Şahin, O. Büyükgüngör, *J. Chin. Chem. Soc.* **2014**, *61*, 1326.
[26] D. A. Köse, H. Necefoglu, H. Icbudak, *J. Coord. Chem.* **2008**, *61*, 3508.

[27] D. A. Köse, A. N. Ay, O. Şahin, O. Büyükgüngör, *J. Iran. Chem. Soc.* **2012**, *9*, 591.
[28] H. Icbudak, Z. Heren, D. A. Kose, H. Necefoglu, *J. Therm. Anal. Calorim.* **2004**, *76*, 837.
[29] D. E. Yıldız, A. Karabulut, I. Orak, A. Turut, *J. Mater. Sci. Mater. Electron.* **2021**, *32*, 10209.
[30] H. H. Gullu, D. E. Yildiz, *J. Mater. Sci. Mater. Electron.* **2020**, *31*, 8705.
[31] M. Yilmaz, A. Kocyigit, B. B. Cirak, H. Kacus, U. Incekara, S. Aydogan, *Mater. Sci. Semicond. Process.* **2020**, *113*, 105039.
[32] N. Suntornwipat, S. Majdi, M. Gabrysch, K. K. Kovi, V. Djurberg, I. Friel, D. J. Twitchen, J. Isberg, *Nano Lett.* **2021**, *21*, 868.
[33] D. E. Yıldız, *J. Mater. Sci. Mater. Electron.* **2018**, *29*, 17802.
[34] S. O. Tan, I. Taşcıoğlu, S. Altındal Yerişkin, H. Tecimer, F. Yakuphanoğlu, *Silicon* **2020**, *12*, 2885.
[35] S. Demirezen, H. G. Çetinkaya, M. Kara, F. Yakuphanoğlu, *Altındal, Sensors Actuators, A Phys.* **2021**, *317*, 112449.
[36] A. Kaya, E. Marıl, Ş. Altındal, İ. Uslu, *Microelectron. Eng.* **2016**, *149*, 166.
[37] A. B. Ulusan, A. Tataroglu, Y. A.-K. Altındal, *J. Mater. Sci. Mater. Electron.* **2021**, *32*, 15732.
[38] Ş. Altındal, Y. Azizian-Kalandaragh, M. Ulusoy, G. Pirgholi-Givi, *J. Appl. Polym. Sci.* **2022**, *139*, e52497.
[39] E. Yükseltürk, O. Surucu, M. Terlemezoglu, M. Parlak, Ş. Altındal, *J. Mater. Sci. Mater. Electron.* **2021**, *32*, 21825.
[40] M. Jaymand, *Prog. Polym. Sci.* **2013**, *38*, 1287.
[41] S. Bhadra, D. Khastgir, N. K. Singha, J. H. Lee, *Prog. Polym. Sci.* **2009**, *34*, 783.
[42] D. E. Yıldız, H. H. Gullu, L. Toppare, A. Cirpan, *J. Mater. Sci. Mater. Electron.* **2020**, *31*, 15233.
[43] X. He, B. Gao, G. Wang, J. Wei, C. Zhao, *Electrochim. Acta* **2013**, *111*, 210.
[44] H. Bejbouj, L. Vignau, J. L. Miane, T. Olinga, G. Wantz, A. Mouhsen, E. M. Oualim, M. Harmouchi, *Mater. Sci. Eng. B Solid-State Mater. Adv. Technol.* **2010**, *166*, 185.
[45] J. L. Alonso, J. C. Ferrer, M. A. Cotarelo, F. Montilla, S. F. de Ávila, *Thin Solid Films* **2009**, *517*, 2729.
[46] V. Talwar, O. Singh, R. C. Singh, *Sens. Actuators B* **2014**, *191*, 276.
[47] E. Song, J. W. Choi, *Microelectron. Eng.* **2014**, *116*, 26.
[48] D. Hazar Apaydin, D. Esra Yildiz, A. Cirpan, L. Toppare, *Sol. Energy Mater. Sol. Cells* **2013**, *113*, 100.
[49] D. E. Yıldız, D. Cevher, M. Yasa, A. Cirpan, L. Toppare, *J. Polym. Sci.* **2022**, *60*, 109.
[50] O. Dayan, A. Gencer Imer, A. G. Al-Sehemi, N. Özdemir, A. Dere, Z. Şerbetçi, A. A. Al-Ghamdi, F. Yakuphanoglu, *J. Mol. Struct.* **2020**, *1200*, 127062.
[51] A. Yeşildağ, *Chem. Pap.* **2021**, *75*, 4949.
[52] B. Barış, M. Yıldırım, S. Karadeniz, A. Karabulut, A. Kose, D. E. Yıldız, *J. Mater. Sci. Mater. Electron.* **2022**, *33*, 2631.
[53] A. Karabulut, D. E. Yıldız, D. A. Köse, M. Yıldırım, *Mater. Sci. Semicond. Process.* **2022**, *146*, 106647.
[54] A. Kocyigit, M. Yıldırım, D. A. Kose, D. E. Yıldız, *Polym. Bull.* **2022**, 1.
[55] D. A. Köse, H. Necefoğlu, O. Şahin, O. Büyükgüngör, *J. Therm. Anal. Calorim.* **2012**, *110*, 1233.
[56] Ö. Dağlı, D. A. Köse, O. Şahin, Z. S. Şahin, *J. Therm. Anal. Calorim.* **2017**, *128*, 1373.
[57] D. A. Köse, B. Zümreoglu-Karan, B. Koşar, O. Büyükgüngör, *J. Chem. Crystallogr.* **2008**, *38*, 305.
[58] D. A. Köse, H. Necefoğlu, *J. Therm. Anal. Calorim.* **2008**, *93*, 509.
[59] M. İlhan, M. M. Koç, B. Coşkun, M. Erkovan, F. Yakuphanoğlu, *J. Mater. Sci. Mater. Electron.* **2021**, *32*, 2346.
[60] M. Raj, C. Joseph, M. Subramanian, V. Perumalsamy, V. Elayappan, *New J. Chem.* **2020**, *44*, 7708.
[61] H. N. Tran, T. A. Bui, G. K. Reeves, P. W. Leech, J. G. Partridge, M. S. N. Alnassar, A. S. Holland, *MRS Adv.* **2016**, *1*, 3655.
[62] A. Kirsoy, M. A. Afrailov, A. Asimov, B. Kucur, *Acta Physica Polonica A*, Polska Akademia Nauk **2015** 170.
[63] L. D. Rao, V. R. Reddy, *AIP Conference Proceedings*, AIP Publishing LLC **2016** 120020.
[64] H. Norde, *J. Appl. Phys.* **1979**, *50*, 5052.
[65] A. Koçyiğit, A. Sarılmaz, T. Öztürk, F. Ozel, M. Yıldırım, *Beilstein J. Nanotechnol.* **2021**, *12*, 984.
[66] T. T. Anh Tuan, D.-H. Kuo, *Mater. Sci. Semicond. Process.* **2015**, *30*, 314.
[67] M. Shkir, M. T. Khan, I. M. Ashraf, A. Almohammedi, E. Dieguez, S. AlFaify, *Sci. Rep.* **2019**, *9*, 1.
[68] C. Li, J. Li, Z. Li, H. Zhang, Y. Dang, F. Kong, *Nanomaterials* **2021**, *11*, 1038.
[69] H. H. Gullu, D. E. Yildiz, A. Kocyigit, M. Yıldırım, *J. Alloys Compd.* **2020**, *827*, 154279.
[70] D. E. Yildiz, H. H. Gullu, A. Sarilmaz, F. Ozel, A. Kocyigit, M. Yildirim, *J. Mater. Sci. Mater. Electron.* **2020**, *31*, 935.
[71] M. Kamruzzaman, J. A. Zapien, *J. Nanosci. Nanotechnol.* **2017**, *17*, 5061.
[72] Y. Wang, S. Yang, A. Ballesio, M. Parmeggiani, A. Verna, M. Cocuzza, C. F. Pirri, S. L. Marasso, *J. Appl. Phys.* **2020**, *128*, 014501.
[73] B. Ezhilmaran, A. Patra, S. Benny, M. R. Sreelakshmi, V. V. Akshay, S. V. Bhat, C. S. Rout, *J. Mater. Chem. C* **2021**, *9*, 6122.
[74] Y. Wang, S. Yang, D. R. Lambada, S. Shafique, *Sensors Actuators, a Phys.* **2020**, *314*, 112232.
[75] J. Jang, D.-M. Geum, S. Kim, *Opt. Express* **2021**, *29*, 38894.
[76] M. Z. Farah Khaleda, B. Vengadaesvaran, N. A. Rahim, *Energy Materials: Fundamentals to Applications*, Elsevier **2021** 525.
[77] L. Hu, J. Yan, M. Liao, L. Wu, X. Fang, *Small* **2011**, *7*, 1012.
[78] L. Li, F. Zhang, J. Wang, Q. An, Q. Sun, W. Wang, J. Zhang, F. Teng, *Sci. Rep.* **2015**, *5*, 1.

How to cite this article: A. Kocyigit, A. A. Hussaini, M. Yıldırım, D. A. Kose, D. E. Yıldız, *Appl Organomet Chem* **2022**, *36*(11), e6879. https://doi.org/10.1002/aoc.6879